Control of Desynchronization Transitions in Delay-Coupled Networks of Type-I and Type-II Excitable Systems

Eckehard Schöll[1], Judith Lehnert[1], Andrew Keane[1], Thomas Dahms[1], and Philipp Hövel[1,2]

[1] Technische Universität Berlin, Institut für Theoretische Physik
Hardenbergstr. 36, 10623 Berlin, Germany
[2] Bernstein Center for Computational Neuroscience, Humboldt-Universität zu Berlin
Philippstraße 13, 10115 Berlin, Germany
schoell@physik.tu-berlin.de
http://www.itp.tu-berlin.de/schoell

Abstract. We discuss synchronization and desynchronization transitions in networks of delay-coupled excitable systems. These transitions arise in response to varying the balance of excitatory and inhibitory couplings in a small-world topology. To describe the local dynamics, we use generic models for type-I excitability, which arises close to a saddle-node bifurcation on an invariant cycle (SNIC or SNIPER), and for type-II excitability, which occurs close to a Hopf bifurcation (FitzHugh-Nagumo model). For large delay times both type-I and type-II systems behave in a similar way. This is different for small delay times, where in case of type-I excitability we find novel multiple transitions between synchronization and desynchronization, when the fraction of inhibitory links is increased. In contrast, only a single desynchronization transition occurs for the FitzHugh-Nagumo model (type-II excitability) for all values of the delay time.

Keywords: complex networks, delayed coupling, synchronization, excitatory and inhibitory balancing, type-I and type-II excitability, small-world

1 Introduction

The control of the dynamics on complex networks has recently gained much interest within the interdisciplinary field of control of nonlinear dynamical systems [1]. Synchronization phenomena in networks are of great importance [2–5] in many areas ranging from physics and chemistry to biology and engineering. Chaos synchronization of lasers, for instance, may lead to new secure communication schemes [6–8]. The synchronization of neurons is believed to play a crucial role in the brain under normal conditions, for instance in the context of cognition, perception, and learning [9–12], and under pathological conditions such as epilepsy

A. Pelster and G. Wunner (eds.), *Selforganization in Complex Systems: The Past, Present, and Future of Synergetics*, Understanding Complex Systems,
DOI: 10.1007/978-3-319-27635-9_3

[13] and Parkinson's disease [14]. Time-delay effects are a key issue in realistic networks. For example, the finite propagation time of light between coupled semiconductor lasers [15–19] significantly influences the dynamics. Similar effects occur in neuronal [20–23] and biological [24, 25] networks. The importance of the effect of delay on synchronization in neural networks was already pointed out by Hermann Haken in his early pioneering work on brain dynamics [26, 9]. There exist different forms of synchronization, i.e., complete or isochronous (zero-lag) synchronization, generalized synchronization, cluster or group synchronization, and many other forms. Chimera states, where a network of identical oscillators splits into distinct coexisting domains of coherent (phase-locked) and incoherent (desynchronized) behavior, have gained much attention recently [27–34].

To determine the stability of a synchronized state in a network of identical units, a powerful method has been developed [35], i.e., the master stability function (MSF). This approach has been extended to networks with coupling delays [36–41], where the MSF depends non-trivially on delay times.

In this chapter we review recent work on synchronization and desynchronization transitions in delay-coupled networks and how they are influenced by the ratio between the number of excitatory and inhibitory links [42, 43]. The issue of balancing excitation and inhibition in neuronal networks has recently found great interest in the neurodynamics community [44–47]. In general, the stability of synchronization depends in a complicated way on the local dynamics of the nodes and the coupling topology. However, for large coupling delays synchronizability relates in a simple way to the spectral properties of the network topology, characterized by the eigenvalue spectrum of the coupling matrix. The MSF used to determine the stability of synchronous solutions has a universal structure in the limit of large delay: it is rotationally symmetric and increases monotonically with the radius in the complex plane. This allows for a universal classification of networks with respect to synchronization properties [39]. For smaller coupling delays the synchronization properties depend in a more subtle way upon the local dynamics, and the details of the network topology. Various cluster-synchronization states, where certain clusters inside the network show isochronous synchronization, can be realized by tuning the coupling parameters such as the coupling phase, coupling strength, and delay time [37, 41]. To find appropriate values of these control parameters, the speed-gradient method from control theory can be applied to achieve a desired state of generalized synchrony (*adaptive synchronization*) [48].

We consider two generic types of local dynamics of the nodes, namely type-I excitable dynamics (near a saddle-node bifurcation on an invariant cycle, or *saddle-node infinite period* (SNIPER) bifurcation), and type-II excitable dynamics (near a Hopf bifurcation, described, e.g., by the FitzHugh-Nagumo model). Transitions between synchronization and desynchronization can be induced by introducing inhibitory links into a regular excitatory network with a probability p, and by changing the balance between excitatory and inhibitory links [42, 43]. The type of network we primarily focus on in our investigations is the small-world (SW) network [49], which has a short average path distance between nodes, as

well as a large degree of clustering (in other words, many triangles in the network structure). These properties are found in many kinds of real-world structures, such as the collaboration between film actors, power grids, the World Wide Web and social relationships [49, 50, 3, 4]. In particular, large-scale cortical networks also show these properties [51, 52]. The brain has an architecture enabling both efficient global and local communication between neurons [53], which is captured well by the SW model.

Inhibition plays an important role in the nervous system [54]. Here, when constructing a network we begin with a regular ring network of excitatory links and, as in Ref. [42, 43], we add long-range inhibitory links into the network structure. This creates a SW network of the form proposed in Ref. [55].

In the following section, we introduce the model and the network topologies considered in the present study. In Sec. 3 we use the master stability function to investigate the stability of arbitrary synchronized networks with given coupling parameters (i.e. the coupling strength and the length of delay between coupled nodes). The MSF is calculated in Sec. 4 for networks coupled within a range of small delay time and coupling strength, which reveals the existence of synchronized states that have different stability conditions compared to coupling with larger delay times. The implications these results may have for specific complex networks are discussed in Sec. 5.

2 Models

In order to model excitability, the system must have a rest state, which corresponds to a stable fixed point. Small perturbations from the rest state can lead to a large excursion in the phase space, i.e., the emission of a spike (excited state), before returning to the rest state. In the context of neurodynamics, this is the firing state of the neuron [56].

Neurons can exhibit different excitability properties, depending upon the bifurcation scenario from the excitable to the oscillatory regime. In 1948, Hodgkin classified two types of neural excitability [57]:

Type-I neurons can generate action potentials of arbitrarily low frequency. This kind of behavior occurs near a saddle-node infinite period (SNIPER) bifurcation, also known as the SNIC bifurcation (saddle-node bifurcation on invariant cycle). The arbitrarily low frequency coincides with the period of the limit cycle going to infinity as the bifurcation parameter approaches a critical value, where the bifurcation occurs.

Type-II neurons are associated with a supercritical Hopf bifurcation. The frequencies of the action potentials remain within a certain non-zero range, while the amplitude of the limit cycle approaches zero with the bifurcation parameter.

As our model for type-I excitability we consider a generic normal form of a SNIPER bifurcation:

$$\mathbf{f}(\mathbf{x}) = \begin{pmatrix} \dot{x} \\ \dot{y} \end{pmatrix} = \begin{pmatrix} x(1-x^2-y^2) + y(x-b) \\ y(1-x^2-y^2) - x(x-b) \end{pmatrix}, \tag{1}$$

which reads in polar coordinates ($x = r\cos\varphi, y = r\sin\varphi$):

$$\dot{r} = r\left(1 - r^2\right) \tag{2}$$

$$\dot{\varphi} = b - r\cos\varphi. \tag{3}$$

$b > 0$ is the bifurcation parameter that influences the type of dynamics and determines where in the (x, y)-plane the fixed points are located, as discussed below. This model was used by Haken and coworkers [58, 59] for the first demonstration of coherence resonance [60], which occurs in excitable nonlinear systems if noise is added; it denotes the counterintuitive effect that the coherence of noise-induced oscillations is optimal for a certain finite noise intensity. Combining this effect with time-delayed feedback, the coherence resonance can be conveniently controlled [61, 62].

Here we focus on the deterministic dynamics of excitable elements (neurons) coupled with time delay τ in a network. We consider the dynamics of a network of N elements (labelled $i = 1, ..., N$) given by:

$$\dot{\mathbf{x}}_i = \mathbf{f}(\mathbf{x}_i) + \sigma \sum_{j=1}^{N} G_{ij}\mathbf{H}(\mathbf{x}_j(t-\tau) - \mathbf{x}_i(t)), \tag{4}$$

where $\mathbf{f}(\mathbf{x}_i)$ is the local dynamics as described by Eq. (1) for each element $\mathbf{x}_i = (x_i, y_i)$. G_{ij} determines the matrix $\mathbf{G}$ for the network structure, showing which elements are coupling together, and $\mathbf{H}$ is the coupling function. $\mathbf{H}$ is taken to be the 2×2 identity matrix; this means that the x-variable at time t is coupled with the x-variable at time $t - \tau$, the y-variable at time t is coupled with the y-variable at time $t - \tau$, but there is no cross-coupling between the x- and y-variable. The coupling parameters, which are identical for all connections, are the coupling strength σ and delay time τ.

For synchronous dynamics, the $2(N-1)$ constraints $\mathbf{x}_s \equiv \mathbf{x}_1 = \mathbf{x}_2 = \cdots = \mathbf{x}_N$ define a 2-dimensional synchronization manifold (SM) within the $2N$-dimensional phase space and the coupled system is reduced to an effective single system with feedback:

$$\dot{\mathbf{x}}_s = \mathbf{f}(\mathbf{x}_s) + \sigma\mathbf{H}(\mathbf{x}_s(t-\tau) - \mathbf{x}_s(t)), \tag{5}$$

with unity row sum $\sum_j G_{ij} = 1$, so that the nodes all receive the same level of input while they are synchronized. Any non-unity but constant row sum can be rescaled using the coupling strength σ.

Without delay, while the bifurcation parameter $b < 1$, there exists an unstable focus at the origin, as well as a saddle point and a stable node situated on the unit circle at $(x_i, y_i) = (b, \sqrt{1-b^2})$ and $(b, -\sqrt{1-b^2})$, respectively. At $b = 1$ the saddle point and stable node collide, so that for $b > 1$ a limit cycle exists along the unit circle. In the case of $b < 1$ (excitable regime), a perturbation which pushes the system from the stable node beyond the saddle point can result in a single oscillation along the unit circle. Delayed coupling can induce a homoclinic bifurcation, such that a limit cycle is produced that bypasses the

saddle point and stable node [61, 62]. Here, we will consider the excitable regime with $b = 0.95$ and investigate for which topologies the synchronized dynamics of complex networks is stable.

Next, as a paradigmatic model for type-II excitability we consider the Fitz-Hugh-Nagumo (FHN) model [63, 64], which exhibits a supercritical Hopf bifurcation:

$$\mathbf{f}(\mathbf{x}) = \begin{pmatrix} \epsilon\dot{x} \\ \dot{y} \end{pmatrix} = \begin{pmatrix} x_i - \frac{x_i^3}{3} - y_i \\ x_i + a \end{pmatrix}, \tag{6}$$

where x and y denote the activator and inhibitor variables, respectively. The parameter a determines the threshold of excitability. A single FHN oscillator is excitable for $a > 1$ and exhibits self-sustained periodic firing beyond the Hopf bifurcation at $a = 1$. Here, we will focus on the excitable regime with $a = 1.3$. The time-scale parameter ϵ is chosen as $\epsilon = 0.01$. The coupling function $\mathbf{H}$ is chosen with components $H_{11} = 1/\epsilon$ and zero otherwise.

In this chapter, complex small-world (SW) networks are considered, which we construct as a variation to the method proposed in Ref. [49], introduced in Refs. [55, 65]: (i) Each of the N nodes in a one-dimensional ring is given excitatory links to its k nearest neighbors on each side. Note that in terms of the matrix $\mathbf{G}$, an excitatory link between the i^{th} and j^{th} node means that $G_{ij} > 0$, while for an inhibitory link $G_{ij} < 0$. (ii) For each of the kN links we add with a probability of p another inhibitory link with strength -1 between two randomly chosen nodes (i.e. on average pkN randomly distributed inhibitory links). (iii) Self-coupling and multiple links between the same two nodes are not allowed. (iv) Finally, the entries in each row of $\mathbf{G}$ are normalized to ensure a unity row sum. If a row sum is equal to zero, then the network realization is discarded.

In the following, we determine the stability of the synchronized dynamics and compare the synchronization/desynchronization transitions for different local dynamics.

3 Stability of Synchronization

In the master stability approach [35], the stability of a synchronized state is determined by splitting the stability problem into a topological part, which is determined by the eigenvalues of the coupling matrix $\mathbf{G}$, and a dynamical part, which is given for an arbitrary network by the master stability equation

$$\delta\dot{\mathbf{x}}(t) = [D\mathbf{f}(\mathbf{x}_s) - \sigma\mathbf{H}]\delta\mathbf{x}(t) + (\alpha + i\beta)\mathbf{H}\delta\mathbf{x}(t - \tau), \tag{7}$$

which is found by linearizing Eq. (4) around Eq. (5) and is used to calculate the largest Lyapunov exponent $\Lambda(\alpha, \beta, \sigma, \tau)$, called the master stability function (MSF). Here $\delta\mathbf{x}$ is the perturbation of $\mathbf{x}$ away from the SM (i.e. $\mathbf{x} = \mathbf{x}_s + \delta\mathbf{x}$) and $D\mathbf{f}(\mathbf{x}_s)$ is the Jacobian matrix of Eq. (1) evaluated on the SM. Important for this approach is that, whereas one can calculate Lyapunov exponents for a specific network topology using the eigenvalues of the matrix $\mathbf{G}$, one considers here a continuous complex parameter $\alpha + i\beta$ representing the complex plane of

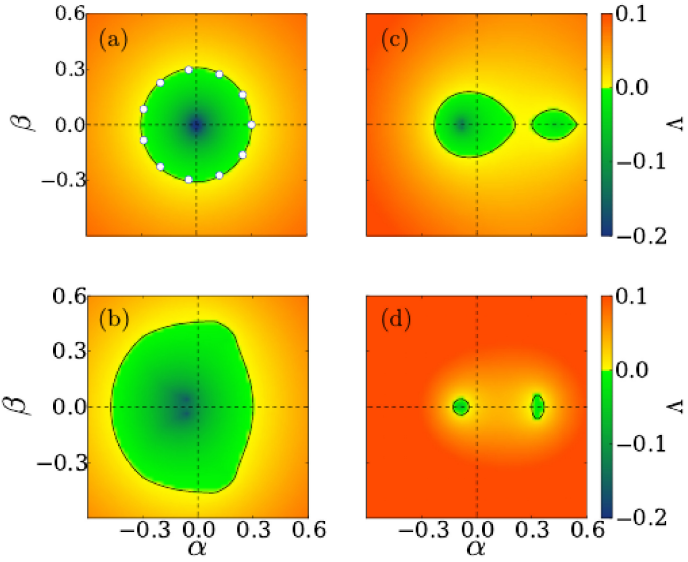

Fig. 1. MSF Λ for the SNIPER model (type-I excitability) for coupling parameters $\sigma = 0.3$ and (a) $\tau = 10$, (b) $\tau = 7$, (c) $\tau = 6.5$, and (d) $\tau = 6$. α and β are the real and imaginary parts of the scaled eigenvalues of the coupling matrix, $\sigma\nu_k$, respectively, and Λ is the largest Lyapunov exponent. White dots in panel (a) represent the scaled eigenvalues of a unidirectional ring of 11 nodes $(\sigma\nu_1, \ldots, \sigma\nu_{11})$. $b = 0.95$.

possible eigenvalues scaled by the coupling strength σ (i.e. $\alpha + i\beta$ is a continuous parametrization of $\sigma\nu_j$, where ν_j are the eigenvalues of $\mathbf{G}, j = 1, ..., N$). Thus, one can calculate the Lyapunov exponents for a region of the (α, β)-plane which gives sub-regions of stability, where $\Lambda < 0$, and instability, where $\Lambda > 0$. It is then easy to compare the synchronous stability of various networks by simply observing whether any of their eigenvalues fall inside an unstable region of the (α, β)-plane. If all the eigenvalues lie within stable regions, then perturbations away from the SM will decay exponentially.

Because of the unity row sum condition, $\mathbf{G}$ always has an eigenvalue $\nu_1 = 1$. This longitudinal eigenvalue (all others are called transversal) corresponds to perturbations within the SM and $\Lambda(\sigma\nu_1, 0, \sigma, \tau)$ is always zero because we are looking at periodic dynamics. As such, it is only the transversal eigenvalues that are important for determining the stability of synchronization.

Figure 1(a) shows the MSF of the SNIPER model (type-I excitability) with coupling parameters $\sigma = 0.3$ and $\tau = 10$. The white dots represent the eigenvalues of the matrix $\mathbf{G}$ for a unidirectional ring of 11 nodes. All eigenvalues are within the stable region of the MSF, thus the synchronization of all 11 nodes coupled with these parameters is stable.

According to Ref. [39], for τ in the order of the system's characteristic time scale (in this case, the period of the oscillations) and above, the MSF will always tend towards a rotational symmetry. Examples such as the one above in Fig. 1(a) confirm these general findings for the SNIPER model. When calculating MSFs for a large fixed τ while varying σ it becomes evident that the size of the stable region is scaled by σ, so that the stable region can be estimated very well by the circle $S((0,0),\sigma)$ (that is, a circle centered at the origin with a radius σ). Changes in large values of τ, however, despite influencing the Lyapunov exponents quantitatively, do not affect the shape of the stable region.

This rotational symmetry of the MSF was also found for type-II neurons, modelled as FitzHugh-Nagumo oscillators by Eq.(6) [42], see Fig. 2. In this case σ and τ do not affect whether the eigenvalues fit into the stable region of the MSF, so that only the topology of a network is important for the stability of its synchronization. Furthermore, because Gershgorin's circle theorem [66] guarantees that the eigenvalues of a network's coupling matrix with no self-coupling and purely excitatory coupling (i.e. $G_{ii} = 0$ and $G_{ij} \geq 0, 1 \leq i, j \leq N$) lie within the unit circle on the complex plane, the synchronization of such a network will always be stable. Finally, if additional inhibitory links are introduced with probability p to construct a SW network as described in Sec. 2, phase transitions from stable to unstable synchronization are found with increasing probability of inhibition p [42]. It should be noted from a comparison of Figs. 1 and 2 that all these results apply for the SNIPER neurons only with sufficiently large τ.

As an example, Fig. 3 shows two realizations of the SW coupling scheme with $N = 20$, $k = 2$, and $p = 0.05$ (panels (a) and (b)) and the corresponding eigenvalues of the coupling matrix depicted in the plot of the MSF in the complex (α, β)-plane (panels (c) and (d)). It can be seen that in panel (c) all eigenvalues lie in the stability domain, and hence synchronization is stable, whereas in panel (d) one eigenvalue lies outside the stability domain, leading to desynchronization. A statistical analysis for a large number of realizations can predict transitions from stable synchronization to desynchronization, as will be discussed in detail in Sec. 5 below.

4 Small delay times

If the delay time is not large enough, type-I excitability (SNIPER model) displays a distinctly different behavior than type-II excitability (FHN model): the rotational symmetry of the MSF no longer holds. In fact, while reducing τ one can witness how the rotational symmetry begins to break down. This is depicted in Fig. 1. For a constant coupling strength of $\sigma = 0.3$, the MSFs are numerically calculated for decreasing delay times. While at $\tau = 10$ the MSF still has its circular form (Fig. 1(a)), when decreasing τ, the stable (i.e. dark blue/green) region of the MSF begins to show signs of deformation. By $\tau = 7$ (see Fig. 1(b)) the stable region is clearly larger than the unit circle scaled by $\sigma = 0.3$ and has definitely lost its rotational symmetry. By $\tau = 6.5$ (see Fig. 1(c)) the stable region has already split into two disconnected regions. Letting τ decrease further,

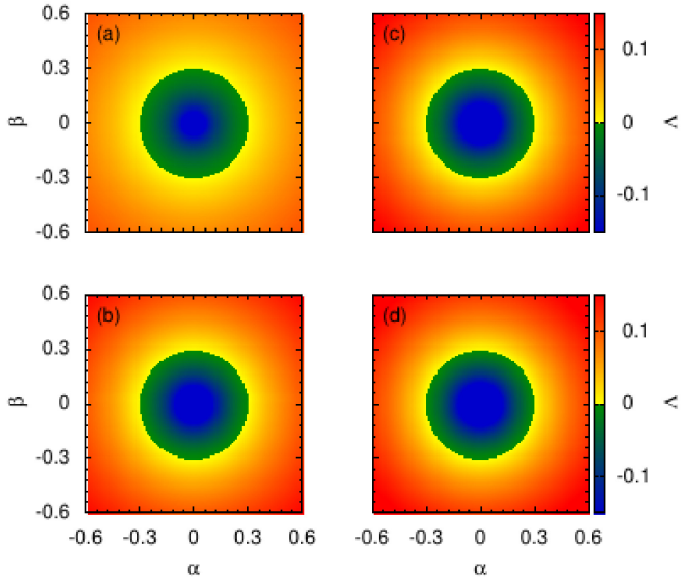

Fig. 2. Same as in Fig. 1 for the FitzHugh-Nagumo model (type-II excitability, $a = 1.3$, $\epsilon = 0.01$) for coupling parameters $\sigma = 0.3$ and (a) $\tau = 10$, (b) $\tau = 7$, (c) $\tau = 6.5$, and (d) $\tau = 6$.

the stable regions become increasingly smaller (see Fig. 1(d)). Note that the delay-induced limit cycle coexists alongside the stable fixed point and whether it is reached or not is therefore dependent on initial conditions. For τ less than about 4 (not shown here), the coupling is no longer able to induce the homoclinic bifurcation that creates the limit cycle at all (as discussed in Sec. 2), in other words, the neurons no longer oscillate. Instead, all solutions approach the stable fixed point.

It is now obvious that, in this regime of small delay, small changes in τ can have a great impact on the stability. The seemingly sudden change in the MSFs in Fig. 1 between $\tau = 7$ and $\tau = 6.5$ can be traced back to a qualitative change at a critical value τ_c, which will be discussed below. Except for this value, the boundary of stability evolves continuously with τ. This becomes clear by plotting the MSF versus the real part α of the eigenvalue (with $\beta = 0$) for varying τ. Taking this one slice of the eigenvalue plane gives a good indication of the growth and decay of the stable region in the MSF while changing τ. Figure 4 shows the MSF as a function of the real part α ($\beta = 0$) and the delay time τ, with fixed coupling strength 0.3. This produces a MSF on an (α, τ)-plane, which can be used for network topologies with a coupling matrix that yields real eigenvalues,

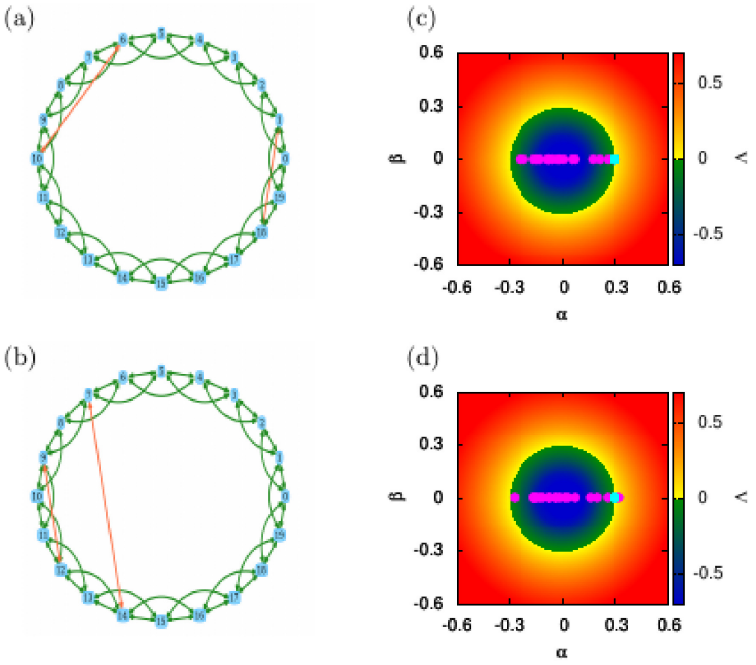

Fig. 3. Synchronization and desynchronization in a small-world network ($\sigma = 0.3$, $\tau = 1$): (a) and (b) are two different realizations with $N = 20$, $k = 2$, and $p = 0.005$. (c),(d): Master stability function Λ of the FitzHugh-Nagumo system ($a = 1.3$, $\epsilon = 0.01$). Dark gray (pink) circles in (c) and (d) mark transversal eigenvalues of the networks shown in panels (a) and (b), respectively; light gray (turquoise) circle: longitudinal eigenvalue.

e.g., symmetric matrices for undirected networks. In the following we restrict ourselves to undirected networks.

The stability depends on both σ and τ. In Fig. 4 the vertical boundary line at $\alpha = \sigma$, corresponding to the longitudinal eigenvalue (i.e. $\nu_1 = 1$, where $\Lambda = 0$), can be easily identified. It separates regimes of stable and unstable synchronization. Another characteristic is that the τ-dependent MSF has a critical delay time τ_c at which the stable region splits into two separate, disconnected regions. For values above τ_c the stable region is found to the left of the longitudinal eigenvalue; whereas for values below τ_c there may be one stable region to the right of the longitudinal eigenvalue and one to the left. τ_c seems to be an important value, because it marks the most significant τ-dependent qualitative change in the MSF. Ultimately, the MSF can be divided into three regimes of τ: (i) two or more smaller separate regions of stability exist when $\tau < \tau_c$; (ii) one large region of stability exists when $\tau > \tau_c$; (iii) the MSF has one rotationally sym-

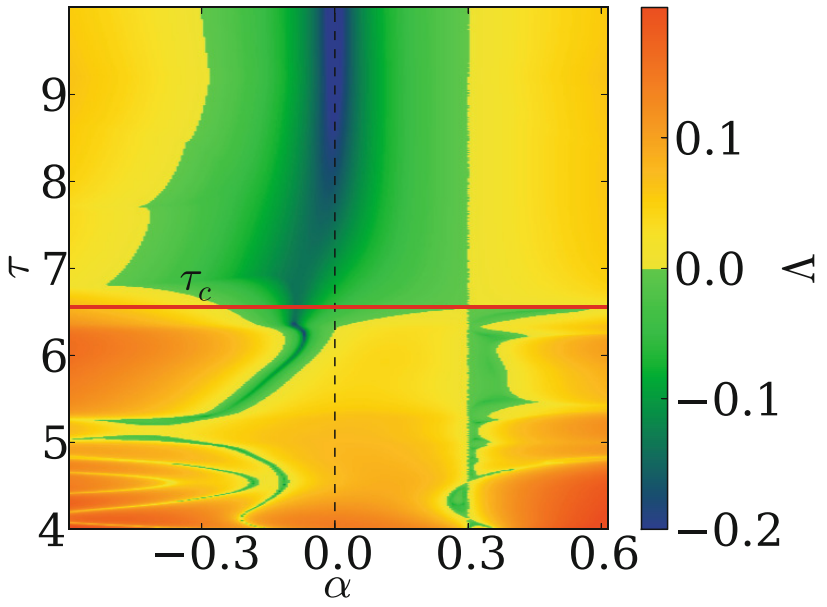

Fig. 4. MSF Λ of the SNIPER model ($b = 0.95$) for a fixed coupling strength $\sigma = 0.3$ in the plane of the real part α ($\beta = 0$) and the delay time τ. The horizontal red line shows the position of the critical delay time τ_c.

metric region of stability in the limit of $\tau \to \infty$ (which holds already in good approximation if τ is of the order of the intrinsic oscillation period or larger).

5 Multiple synchronization and desynchronization transitions

An obvious observation is that networks with purely excitatory coupling, which are always stable for large delay times as mentioned at the end of Sec. 3, may not show stable synchronization for $\tau < \tau_c$. It was explained in Sec. 3 that increasing the probability p of inhibitory links in the network can be a factor leading to unstable synchronization. This occurs because a larger probability of inhibition can push a part of the eigenvalue spectrum of any network beyond the longitudinal eigenvalue at $\alpha = \sigma$ (because Gershgorin's circle theorem no longer guarantees that all eigenvalues stay within the unit circle) and into the unstable region of the MSF. Now, in case of excitability of type-I for smaller τ, there may be a pocket of stability to the right of the longitudinal eigenvalue, so that increasing inhibition can make the otherwise unstable synchronization of a network stable.

This means that the transitions between stable and unstable synchronization as a function of the probability of inhibition p discussed in Ref. [42] are no

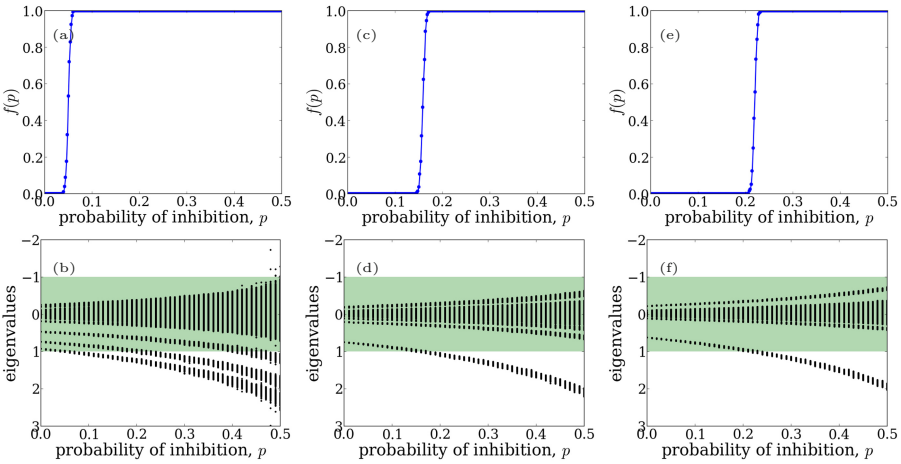

Fig. 5. Fraction of desynchronized networks f in dependence of the probability of additional inhibitory links p for 500 realizations of networks of $N = 200$ with (a) $k = 20$, (c) $k = 40$, and (e) $k = 50$. Corresponding eigenvalue spectra for (b) $k = 20$, (d) $k = 40$, and (f) $k = 50$ with 100 realizations for each p value. Here the green shaded regions represent the stable regions of the real part of the MSF typical for the SNIPER model for large delay and for the FitzHugh-Nagumo system for both small and large delay.

longer valid when τ is small in case of type-I excitability. The transitions are now sensitive to the coupling parameters, not just the network parameters N and k. Due to the multiple regions of stability, eigenvalues may wander in and out of stable regions, while increasing the probability of inhibition p. For large τ, or for any τ in case of type-II excitability, increasing p in the SW network model only results in one transition where the fraction of desynchronizing networks (i.e. networks with unstable synchronization) $f(p)$ switches from 0 to 1 (cf. Fig. 5).

For small τ, in case of excitability of type-I it is possible that $f(p)$ jumps back to 0, before increasing again to 1. This will occur if there is a separate region of stability to the right side in the MSF that is large enough that all the eigenvalues lying over there can fit inside.

The observation of multiple transitions between stable and unstable synchronization can be explained by looking at the eigenvalue spectra for SW networks for various p values. As discussed above in relation to the MSF method, each network topology has a coupling matrix $\mathbf{G}$, the eigenvalues from which can be used to determine the stability of the network's synchronized state. Because the "short-cuts" in the SW network are randomly introduced, each network with specific N, k and p values may have many realizations. By calculating the eigenvalues for a large number of realizations of the SW network with certain parameters (i.e. given N, k and p), one can find the bounds for the eigenvalue spectra.

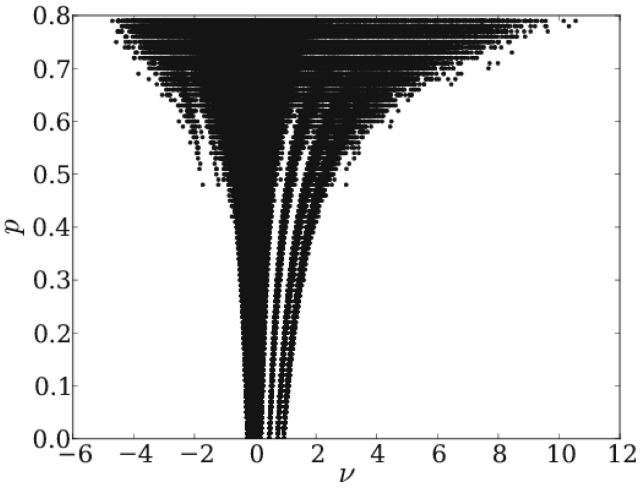

Fig. 6. Spectra of eigenvalues ν of undirected small-world networks with $N = 200$ and $k = 20$ and varying probability p of inhibitory links. 500 realizations of the eigenvalue spectrum are plotted for each value of p.

Figure 6 displays the superimposed eigenvalue spectra of 500 realizations for SW networks with parameters $N = 200$ and $k = 20$ (regular ring with excitatory coupling of k nearest neighbors on either side) in dependence on the probability of inhibition p. The longitudinal eigenvalues located at $\nu_1 = 1$ have been removed. One can see that the bounds for possible eigenvalues shift depending on the value of p. One can also see how the spectra begin to increasingly resemble the semicircular distribution [3] of a random network for larger p values, where the networks have lost their SW properties. The change of the eigenvalue spectrum with increasing p has been discussed in detail elsewhere [43].

The eigenvalue spectra bridge the gap between observations of the MSF (i.e. the dependence of the stability of synchronization on the eigenvalues) and what is seen in these transitions (i.e. the dependence of stability on the network topology). Increasing p allows isolated eigenvalues to increase in value and, in terms of the MSF, shift their locations further to the right in the (α, β)-plane. This is visualized in Fig. 7. Figures 7(b), (d) and (f) show the eigenvalue spectra for SW networks with $N = 200$ elements and $k = 20$, 40, and 50, respectively.

Figures 7(a), (c) and (e) show the corresponding fraction of desynchronized networks f in dependence on the probability of additional inhibitory links p. Consider, for instance, SW networks with parameters $N = 200$ and $k = 40$. In Fig. 7(c) $f(p)$ is shown for the exemplary coupling parameters $\sigma = 0.3$ and $\tau = 6.5$ with a corresponding plot of eigenvalues in Fig. 7(d). Note that the grey (green) shaded regions represent the stable regions of the line $\beta = 0$ on the (α, β)-plane of the MSF for $\sigma = 0.3$ and $\tau = 6.5$ (cf. Fig. 1(c)). For coupling parameters

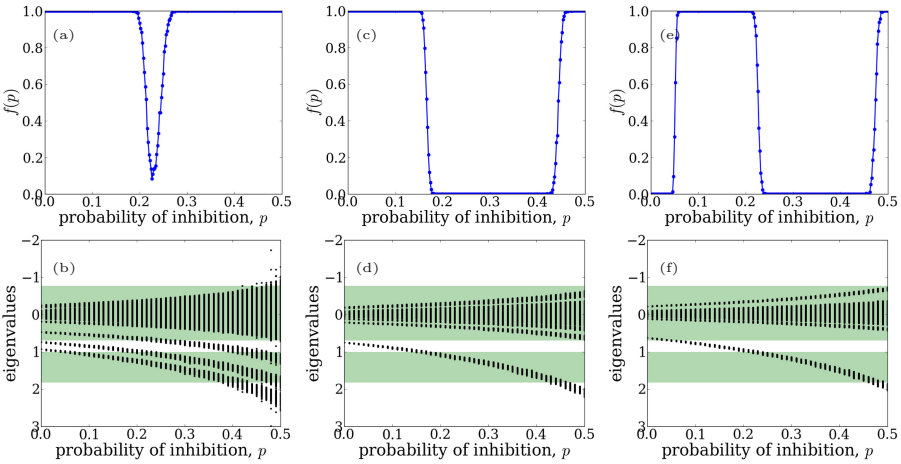

Fig. 7. Fraction of desynchronized networks f in dependence of the probability of additional inhibitory links p for 500 realizations of networks of $N = 200$ with (a) $k = 20$, (c) $k = 40$, and (e) $k = 50$ with $\sigma = 0.3$ and $\tau = 6.5$. Corresponding eigenvalue spectra for (b) $k = 20$, (d) $k = 40$, and (f) $k = 50$ with 100 realizations for each p value. Here the green shaded regions represent the stable regions of the real part of the MSF of the SNIPER model ($b = 0.95$).

where this region of stability is not large enough, f may briefly dip below 1 without decreasing to 0, because only some realizations may have eigenvalues that fit inside the stable region. In Fig. 7(a) where $k = 20$, f dips down to 0.14, because at most 14% of the realizations show stable synchronization (i.e. all the eigenvalues are inside the stable region). If the distance between the larger isolated eigenvalues matches the distance between stable regions (which is almost the case in Fig. 7(b)), then the transition curve only just touches the $f = 0$ axis at some value of p before increasing back to $f = 1$. Figure 7(e) is an example where a further transition is possible, because not only do all eigenvalues begin in stable regions at $p = 0$, but there is another regime of p where all eigenvalues fit inside stable regions. Note that further types of transitions can also occur for other network and coupling parameters.

The length of the transition from $f = 0$ to $f = 1$ is actually a measure of the variance of the isolated eigenvalues for an ensemble of realizations. For example, the variance of the isolated eigenvalues decreases as N is increased, so that the length of transition will be shorter in larger networks, and the transition becomes sharper.

When constructing a histogram of the eigenspectra for a particular value of p, the larger isolated eigenvalues seen to the right, e.g., in Fig. 7(b), result in small peaks of eigenvalues. See Fig. 8(a) for 1000 realizations of $p = 0.2$. For each realization of many SW networks there are isolated eigenvalues that are larger than most other eigenvalues in the spectrum. The small peaks of eigenvalues result from perturbations in isolated eigenvalues. For comparison, Fig. 8(b) shows

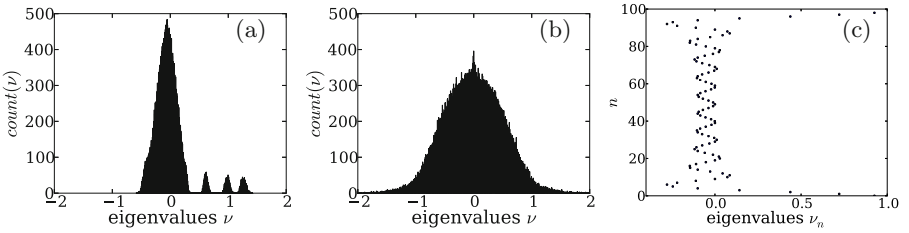

Fig. 8. (a), (b): Histograms (1000 bins) of eigenvalue spectra for 1000 realizations of (a) SW networks and (b) random networks with the same number of nodes, the same number of excitatory links and the same probability of inhibitory links ($N = 100$, $k = 10$, $p = 0.2$). (c): The eigenvalue spectrum for a regular network with $N = 100$ and $k = 10$. ν_n is the n^{th} eigenvalue, $n = 1, \ldots, N$.

the reference case of 1000 random networks with the same number of nodes and excitatory links and the same probability of inhibitory links as considered in Fig. 8(a).

The spectrum of a regular ring network, i.e., a SW network with $p = 0$, can be found analytically using the graph's symmetry operations [67] and is given by

$$\nu_l = \frac{1}{k}\sum_{j=1}^{k}\cos\left(2\pi j\frac{l}{N}\right) = \frac{1}{k}\left(\frac{\cos\left(k\pi\frac{l}{N}\right)\sin\left((k+1)\pi\frac{l}{N}\right)}{\sin\left(\pi\frac{l}{N}\right)} - 1\right), \qquad (8)$$

where $l = 1, ..., N-1$. Figure 8(c) shows this eigenspectrum for the $p = 0$ case. As p is increased these eigenvalues will be slightly perturbed (in a random manner) by the changing network structure, of which many realizations are possible. The isolated eigenvalues to the right-hand side in Fig. 8(c) eventually evolve into the smaller side peaks of eigenvalues in histograms for larger p as depicted in Fig. 8(a) for $p = 0.2$. These peaks show the distribution of the eigenvalue under the influence of the random nature of the SW "short-cuts" creation process – which is why the smaller eigenvalue peaks can be approximated by a normal distribution. To be precise, because the multiplicity of the above mentioned isolated eigenvalues at $p = 0$ is 2, the smaller eigenvalue peaks are two normal distributions that, at least for small p values, overlap each other to a large extent. This is furthermore the reason why the desynchronization transitions observed in Ref. [42] and Figs. 7(a), (c), and (e) look like the cumulative (integrated) distribution function. They reflect how an increase of p brings the area of the small eigenvalue peak accumulatively into the unstable region of the MSF.

To explain why the peaks wander with increasing p, consider not normalizing the rows of matrix $\mathbf{G}$, so that the row sums are not necessarily equal to 1. Then the location of the longitudinal eigenvalue decreases with p, because it is equal to the average row sum of $\mathbf{G}$ given by $2k(1-p)$. The locations of the other peaks increase slightly to maintain the eigenvalue sum of zero; a result of the trace of $\mathbf{G}$ being zero, since there is no self-feedback coupling. For large N this has only

a small effect. Thus, scaling the eigenvalues so that the longitudinal eigenvalue is always at 1 means that the transversal eigenvalues are multiplied by $\frac{1}{2k(1-p)}$. Accordingly they appear to increase with p, as seen in Figs. 7(b), (d) and (f).

6 Conclusion

We have investigated transitions between synchronization and desynchronization in complex networks of delay-coupled excitable elements of type I and type II, induced by varying the balance between excitatory and inhibitory couplings in a small-world topology. In our analysis we have used the master stability function approach. For large delay times it seems that both type-I neurons and type-II neurons must fulfill similar topological conditions in the network to allow for a stable synchronized state. This is different when considering small delay times. In case of the SNIPER model (type-I excitability), for a range of small coupling strengths and small delay times we have found novel multiple transitions between synchronization and desynchronization, when the fraction of inhibitory links is increased. This is different for the FitzHugh-Nagumo model (type-II excitability), where only a single transition from synchronization to desynchronization occurs for all values of the delay time. This can be explained by the different nature of the stability domains of the master stability function which consists of disconnected stability islands in case of type-I excitability for small τ. A small world model for complex networks with regular excitatory couplings and random inhibitory shortcuts has eigenvalue spectra with gaps between the larger eigenvalues, so that histograms of many realizations reveal isolated peaks of possible eigenvalues. Synchronization occurs whenever the domains of the eigenvalues fall onto the stability islands. It was shown that, because of this, small world networks can go through multiple transitions of synchronization and desynchronization in dependence on the probability of inhibitory short-cuts for the model of type-I excitability. Note that the same has also been shown for the Stuart-Landau model in Ref. [43], demonstrating that multiple transitions can also appear in networks of oscillatory nodes and are not limited to excitable systems.

Acknowledgments. This work was supported by the DFG in the framework of the SFB 910. PH acknowledges support by the BMBF (grant no. 01GQ1001B).

References

1. Schöll, E., Schuster, H.G. (eds.): Handbook of Chaos Control. Wiley-VCH, Weinheim (2008), second completely revised and enlarged edition
2. Pikovsky, A.S., Rosenblum, M.G., Kurths, J.: Synchronization. A Universal Concept in Nonlinear Sciences. Cambridge University Press, Cambridge (2001)
3. Albert, R., Barabási, A.-L.: Statistical mechanics of complex networks. Rev. Mod. Phys. **74**, 47 (2002)

4. Newman, M.E.J.: The structure and function of complex networks. SIAM Review **45**, 167 (2003)
5. Boccaletti, S., Latora, V., Moreno, Y., Chavez, M., Hwang, D.U.: Complex networks: Structure and dynamics. Physics Reports **424**, 175 (2006)
6. Cuomo, K.M., Oppenheim, A.V.: Circuit implementation of synchronized chaos with applications to communications. Phys. Rev. Lett. **71**, 65 (1993)
7. Boccaletti, S., Kurths, J., Osipov, G., Valladares, D.L., Zhou, C.S.: The synchronization of chaotic systems. Phys. Rep. **366**, 1 (2002)
8. Kanter, I., Kopelowitz, E., Kinzel, W.: Public channel cryptography: chaos synchronization and Hilbert's tenth problem. Phys. Rev. Lett. **101**, 84102 (2008)
9. Haken, H.: Brain Dynamics: Synchronization and Activity Patterns in Pulse-Coupled Neural Nets with Delays and Noise. Springer, Berlin (2007)
10. Singer, W.: Neuronal Synchrony: A Versatile Code Review for the Definition of Relations? Neuron **24**, 49 (1999)
11. Engel, A., Fries, P., Singer, W.: Dynamic predictions: Oscillations and synchrony in top-down processing. Nature Reviews Neuroscience **2**, 704 (2001)
12. Melloni, L., Molina, C., Pena, M., Torres, D., Singer, W., Rodriguez, E.: Synchronization of neural activity across cortical areas correlates with conscious perception. J. Neurosci. **27**, 2858 (2007)
13. Traub, R.D., Wong, R.K.: Cellular mechanism of neuronal synchronization in epilepsy. Science **216**, 745 (1982)
14. Tass, P.A., Rosenblum, M.G., Weule, J., Kurths, J., Pikovsky, A.S., Volkmann, J., Schnitzler, A., Freund, H.J.: Detection of n:m phase locking from noisy data: Application to magnetoencephalography. Phys. Rev. Lett. **81**, 3291 (1998)
15. Wünsche, H.J., Bauer, S., Kreissl, J., Ushakov, O., Korneyev, N., Henneberger, F., Wille, E., Erzgräber, H., Peil, M., Elsäßer, W., Fischer, I.: Synchronization of delay-coupled oscillators: A study of semiconductor lasers. Phys. Rev. Lett. **94**, 163901 (2005)
16. Carr, T.W., Schwartz, I.B., Kim, M.Y., Roy, R.: Delayed-mutual coupling dynamics of lasers: scaling laws and resonances. SIAM J. Appl. Dyn. Syst. **5**, 699 (2006)
17. Erzgräber, H., Krauskopf, B., Lenstra, D.: Compound laser modes of mutually delay-coupled lasers. SIAM J. Appl. Dyn. Syst. **5**, 30 (2006)
18. Fischer, I., Vicente, R., Buldú, J.M., Peil, M., Mirasso, C.R., Torrent, M.C., García-Ojalvo, J.: Zero-lag long-range synchronization via dynamical relaying. Phys. Rev. Lett. **97**, 123902 (2006)
19. D'Huys, O., Vicente, R., Erneux, T., Danckaert, J., Fischer, I.: Synchronization properties of network motifs: Influence of coupling delay and symmetry. Chaos **18**, 037116 (2008)
20. Timme, M., Wolf, F., Geisel, T.: Coexistence of regular and irregular dynamics in complex networks of pulse-coupled oscillators. Phys. Rev. Lett. **89**, 258701 (2002)
21. Rossoni, E., Chen, Y., Ding, M., Feng, J.: Stability of synchronous oscillations in a system of Hodgkin-Huxley neurons with delayed diffusive and pulsed coupling. Phys. Rev. E **71**, 061904 (2005)
22. Masoller, C., Torrent, M.C., García-Ojalvo, J.: Interplay of subthreshold activity, time-delayed feedback, and noise on neuronal firing patterns. Phys. Rev. E **78**, 041907 (2008)
23. Englert, A., Heiligenthal, S., Kinzel, W., Kanter, I.: Synchronization of chaotic networks with time-delayed couplings: An analytic study. Phys. Rev. E **83**, 046222 (2011)

24. Takamatsu, A., Tanaka, R., Yamada, H., Nakagaki, T., Fujii, T., Endo, I.: Spatiotemporal symmetry in rings of coupled biological oscillators of physarum plasmodial slime mold. Phys. Rev. Lett. **87**, 078102 (2001)
25. Tiana, G., Jensen, M.H.: The dynamics of genetic control in the cell: the good and bad of being late. Phil. Trans. R. Soc. (2013) (in print)
26. Haken, H.: Effect of delay on phase locking in a pulse coupled neural network. Eur. Phys. J. B **18**, 545 (2000)
27. Kuramoto, Y., Battogtokh, D.: Coexistence of Coherence and Incoherence in Nonlocally Coupled Phase Oscillators. Nonlin. Phen. in Complex Sys. **5**, 380 (2002)
28. Abrams, D.M., Strogatz, S.H.: Chimera states for coupled oscillators. Phys. Rev. Lett. **93**, 174102 (2004)
29. Martens, E.A., Laing, C.R., Strogatz, S.H.: Solvable model of spiral wave chimeras. Phys. Rev. Lett. **104**, 044101 (2010)
30. Motter, A.E.: Nonlinear dynamics: Spontaneous synchrony breaking. Nature Physics **6**, 164 (2010)
31. Omelchenko, I., Maistrenko, Y.L., Hövel, P., Schöll, E.: Loss of coherence in dynamical networks: spatial chaos and chimera states. Phys. Rev. Lett. **106**, 234102 (2011)
32. Omelchenko, I., Riemenschneider, B., Hövel, P., Maistrenko, Y.L., Schöll, E.: Transition from spatial coherence to incoherence in coupled chaotic systems. Phys. Rev. E **85**, 026212 (2012)
33. Hagerstrom, A., Murphy, T.E., Roy, R., Hövel, P., Omelchenko, I., Schöll, E.: Experimental observation of chimeras in coupled-map lattices. Nature Physics **8**, 658 (2012)
34. Tinsley, M.R., Nkomo, S., Showalter, K.: Chimera and phase cluster states in populations of coupled chemical oscillators. Nature Physics **8**, 662 (2012)
35. Pecora, L.M., Carroll, T.L.: Master stability functions for synchronized coupled systems. Phys. Rev. Lett. **80**, 2109 (1998)
36. Dhamala, M., Jirsa, V.K., Ding, M.: Enhancement of neural synchrony by time delay. Phys. Rev. Lett. **92**, 074104 (2004)
37. Choe, C.U., Dahms, T., Hövel, P., Schöll, E.: Controlling synchrony by delay coupling in networks: from in-phase to splay and cluster states. Phys. Rev. E **81**, 025205(R) (2010)
38. Kinzel, W., Englert, A., Reents, G., Zigzag, M., Kanter, I.: Synchronization of networks of chaotic units with time-delayed couplings. Phys. Rev. E **79**, 056207 (2009)
39. Flunkert, V., Yanchuk, S., Dahms, T., Schöll, E.: Synchronizing distant nodes: a universal classification of networks. Phys. Rev. Lett. **105**, 254101 (2010)
40. Heiligenthal, S., Dahms, T., Yanchuk, S., Jüngling, T., Flunkert, V., Kanter, I., Schöll, E., Kinzel, W.: Strong and weak chaos in nonlinear networks with time-delayed couplings. Phys. Rev. Lett. **107**, 234102 (2011)
41. Dahms, T., Lehnert, J., Schöll, E.: Cluster and group synchronization in delay-coupled networks. Phys. Rev. E **86**, 016202 (2012)
42. Lehnert, J., Dahms, T., Hövel, P., Schöll, E.: Loss of synchronization in complex neural networks with delay. Europhys. Lett. **96**, 60013 (2011)
43. Keane, A., Dahms, T., Lehnert, J., Suryanarayana, S.A., Hövel, P., Schöll, E.: Synchronisation in networks of delay-coupled type-I excitable systems. Eur. Phys. J. B **85**, 407 (2012)
44. Vogels, T.P., Abbott, L.F.: Gating multiple signals through detailed balance of excitation and inhibition in spiking networks. Nature Neurosci. **12**, 483 (2009)

45. Vogels, T.P., Sprekeler, H., Zenke, F., Clopath, C., Gerstner, W.: Inhibitory plasticity balances excitation and inhibition in sensory pathways and memory networks. Science **334**, 1569 (2011)
46. Ernst, U., Pawelzik, K.: Sensible balance. Science **334**, 1507 (2011)
47. Hennequin, G., Vogels, T.P., Gerstner, W.: Non-normal amplification in random balanced neuronal networks. Phys. Rev. E **86**, 011909 (2012)
48. Selivanov, A.A., Lehnert, J., Dahms, T., Hövel, P., Fradkov, A.L., Schöll, E.: Adaptive synchronization in delay-coupled networks of Stuart-Landau oscillators. Phys. Rev. E **85**, 016201 (2012)
49. Watts, D.J., Strogatz, S.H.: Collective dynamics of 'small-world' networks. Nature **393**, 440 (1998)
50. Adamic, L.A.: The small world web, vol. 1696/1999. Lecture Notes in Computer Science. Springer Berlin, Heidelberg (1999)
51. Sporns, O., Tononi, G., Edelman, G.M.: Theoretical Neuroanatomy: Relating Anatomical and Functional Connectivity in Graphs and Cortical Connection Matrices. Cereb. Cortex **10**, 127 (2000)
52. Sporns, O.: Small-world connectivity, motif composition, and complexity of fractal neuronal connections. Biosystems **85**, 55 (2006)
53. Latora, V., Marchiori, M.: Efficient behavior of small-world networks. Phys. Rev. Lett. **87**, 198701 (2001)
54. Haider, B., Duque, A., Hasenstaub, A.R., McCormick, D.A.: Neocortical network activity in vivo is generated through a dynamic balance of excitation and inhibition. J. Neurosci. **26**, 4535 (2006)
55. Newman, M.E.J., Watts, D.J.: Renormalization group analysis of the small-world network model. Phys. Lett. A **263**, 341 (1999)
56. Izhikevich, E.M.: Neural excitability, spiking and bursting. Int. J. Bifurcation Chaos **10**, 1171 (2000)
57. Hodgkin, A.L.: The local electric changes associated with repetitive action in a medullated axon. J. Physiol. **107**, 165 (1948)
58. Hu, G., Ditzinger, T., Ning, C.Z., Haken, H.: Stochastic resonance without external periodic force. Phys. Rev. Lett. **71**, 807 (1993)
59. Ditzinger, T., Ning, C.Z., Hu, G.: Resonancelike responses of autonomous nonlinear systems to white noise. Phys. Rev. E **50**, 3508 (1994)
60. Pikovsky, A.S., Kurths, J.: Coherence resonance in a noise-driven excitable system. Phys. Rev. Lett. **78**, 775 (1997)
61. Hizanidis, J., Aust, R., Schöll, E.: Delay-induced multistability near a global bifurcation. Int. J. Bifur. Chaos **18**, 1759 (2008)
62. Aust, R., Hövel, P., Hizanidis, J., Schöll, E.: Delay control of coherence resonance in type-I excitable dynamics. Eur. Phys. J. ST **187**, 77 (2010)
63. FitzHugh, R.: Impulses and physiological states in theoretical models of nerve membrane. Biophys. J. **1**, 445 (1961)
64. Nagumo, J., Arimoto, S., Yoshizawa, S.: An active pulse transmission line simulating nerve axon. Proc. IRE **50**, 2061 (1962)
65. Monasson, R.: Diffusion, localization and dispersion relations on"small-world" lattices. Eur. Phys. J. B **12**, 555 (1999)
66. Gerschgorin, S.A.: Über die Abgrenzung der Eigenwerte einer Matrix. Izv. Akad. Nauk. SSSR **7**, 749 (1931)
67. Farkas, I., Derenyi, I., Barabási, A.-L., Vicsek, T.: Spectra of real-world graph: Beyond the semicircle law. Phys. Rev. E **64**, 026704 (2001)